

# Computerized craniofacial reconstruction using CT-derived implicit surface representations

Dirk Vandermeulen<sup>a,\*</sup>, Peter Claes<sup>a</sup>, Dirk Loeckx<sup>a</sup>, Sven De Greef<sup>b</sup>,  
Guy Willems<sup>b</sup>, Paul Suetens<sup>a</sup>

<sup>a</sup> *Katholieke Universiteit Leuven, Faculties of Engineering and Medicine, Medical Image Computing, ESAT & Radiology, Herestraat 49, B-3000 Leuven, Belgium*

<sup>b</sup> *Katholieke Universiteit Leuven, Faculty of Medicine, School of Dentistry, Oral Pathology and Maxillo-Facial Surgery, Department of Forensic Odontology, Kapucijnenvoer 7, B-3000 Leuven, Belgium*

Available online 15 March 2006

## Abstract

In forensic craniofacial reconstruction, facial features of an unknown individual are estimated from an unidentified skull, based on a mixture of experimentally obtained guidelines on the relationship between soft tissues and the underlying skeleton. In this paper, we investigate the possibility of using full 3D cross-sectional CT images for establishing a reference database of densely sampled distances between the external surfaces of the skull and head for automated craniofacial reconstruction. For each CT image in the reference database, the hard tissue (skull) and soft tissue (head) volumes are automatically segmented and transformed into signed distance transform (sDT) images, representing for each voxel in this image the Euclidean distance to the closest point on the skull and head surface, respectively, distances being positive (negative) for voxels inside (outside) the skull/head. Multiple craniofacial reconstructions are obtained by first warping each reference skull sDT maps to the target skull sDT using a B-spline based free form deformation algorithm and subsequently applying these warps to the reference head sDT maps. A single reconstruction of the target head surface is defined as the zero level set of the arithmetic average of all warped reference head sDT maps, but other reconstructions are possible, biasing the result to subject specific attributes (age, BMI, gender). Both qualitative and quantitative tests (measuring the similarity between the 3D reconstructed and corresponding original head surface) on a small ( $N = 20$ ) database are presented to proof the validity of the concept.

© 2006 Elsevier Ireland Ltd. All rights reserved.

*Keywords:* Craniofacial reconstruction; Computer tomography

## 1. Introduction

In forensic pathology, craniofacial reconstructions are sometimes the only way to indirectly infer the identity of a missing person. The purpose of forensic facial reconstruction is to approximate facial features of the unknown individual to aid in recognition and further identification based on additional evidence. All facial reconstruction techniques are based on the assumed relationship between the soft tissue envelope and the underlying skull substrate [1,2]. Traditional ‘plastic’ methods use modelling clay or plasticine to build up the depth of tissue on the dry skull or a cast of the skull, based on a set of anatomy-based rules, combined with some artistic sense. These

procedures are extremely time-consuming (limiting their use to exceptional and/or urgent cases), subjective and result in a single facial estimate being produced. The development of software for computerized facial reconstructions of an individual would be of benefit to various law enforcement agencies, by allowing faster, easier and more efficient generation of multiple representations of an individual. These varied likenesses would take into account differences in facial appearance due to subject-specific attributes such as gender, age and posture augmented with localized facial features such as the eyes, nose and lips, which are difficult to reconstruct accurately solely from cranial information.

The majority of published computerized craniofacial surface reconstruction techniques [3–7] are based on fitting a generic head surface to a set of interactively or automatically placed virtual dowels on a 3D digitized model of the skull. The head and skull surfaces are extracted from 3D computed tomography (CT)

\* Corresponding author. Tel.: +32 16 349022.

E-mail address: [dirk.vandermeulen@esat.kuleuven.be](mailto:dirk.vandermeulen@esat.kuleuven.be) (D. Vandermeulen).

imaging or obtained directly by 3D laser scanning. The dowel lengths represent estimates of tissue thickness at a limited number (20–30) of predefined locations on the skull. These tissue thickness estimates are averages over a certain subclass of individuals defined by ancestry, gender and age. Head surface shape is directly defined at the dowel positions only, and inferred by interpolation in between, possibly in combination with some extra manual modelling of the nose, eyes, e.g. afterwards to improve the result. In an attempt to increase the number of skull points involved in the estimation of soft tissue thickness, a number of computer-based techniques deform a reference skull surface to a target skull surface [8–11]. The calculated skull deformation is extrapolated and applied to the head surface associated to the reference skull in order to estimate the facial outlook corresponding to the target skull. A reference skull is selected based on similarity in ancestry, gender and age. Reference skulls and corresponding facial surfaces are obtained using CT-scanning, which limits the selection of the reference database to patient data because of the involved radiation dose. However, all these reconstructions are biased by the generic head surface or specific best look-alike used. In order to remove this bias, a statistical model of soft tissue thicknesses and facial outlook can be fitted to the individual skull [12,13]. Our work is similar in spirit to [13] in the use of multiple reference head and skull surfaces and to [8–11] in the concept of warping reference skull to target skull and applying this warp to the reference skin. All skull and head surfaces of the reference database can be relatively easily and robustly extracted from volumetric imaging data such as 3D CT-scanning.

Our procedure can be summarized as follows. For each CT image in the reference database, the hard tissue (“skull”) and soft tissue (“head”) are segmented using hysteresis intensity thresholding in combination with morphological operations to remove noisy parts and to close the volumes for subsequent operations. The images corresponding to the volumes encompassed by both surfaces are each transformed into signed distance transform (sDT) maps, representing for each image voxel the shortest Euclidean distance to the nearest surface point, zero on the surface, positive inside and negative outside. As a proof of concept, a simplified procedure for reconstructing the target head surfaces was implemented, by warping all reference skull sDT images to the target skull sDT. These warps are subsequently applied to all the associated reference head sDT maps. Finally, the zero iso-level surface of the arithmetic average of the warped reference head sDT maps is defined as the reconstructed skin surface. Other linear combinations such as mixtures of modes of variation (using principal component decompositions) are possible as well, but require a substantially larger reference database.

## 2. Materials and methods

### 2.1. CT-image acquisition, processing and segmentation

The CT data used in this study were acquired on a 16-slice spiral CT scanner (Somatom Sensation 16, Siemens, Erlangen, Germany) as part of a routine head-and-neck protocol CT

examination ( $N = 13$ ). An additional subset of seven CT data sets were acquired with a clinical-dose total head multi-slice CT-scanning protocol as part of a preoperative osteotomy surgery planning procedure. All images are stored in a Picture Archiving and Communications System (PACS) image database from which they were selectively retrieved on the basis of their quality for reconstruction. On the one hand, the scanned area should at least cover the region extending from slightly below the chin to a few centimetres above the eyebrows. On the other hand, the images should contain only a minimal amount of metal streak artefacts that interfere with a correct segmentation of the head and skull surface.

All images originally stored in DICOM format are converted to Analyze (Mayo Foundation, Rochester, MN, USA) image format and down-sampled for computational efficiency by a factor of 2 in each dimension, resulting in image sizes of approximately  $256 \times 256 \times 200$  unsigned integers (voxel sizes  $\approx 0.7 \text{ mm} \times 0.7 \text{ mm} \times 1 \text{ mm}$ ). Any remaining streak artefacts due to the amalgam teeth fillings are reduced using a simplified version of a projection interpolation method [14]. The head volume is segmented by intensity thresholding at 300 HU (Hounsfield units), followed by a morphological opening with a sphere with a radius of 2 voxels to remove isolated artefacts and a final hole filling, to obtain a solid volume  $\Omega_H$ , represented by the binary image  $H(x)$  defined as:  $H(x) = 1$ , if  $x \in \Omega_H$ , and 0 otherwise, for every voxel  $x$ . Bone is segmented by hysteresis thresholding [15] in the range [1000–1500] HU, followed by morphological closing with a sphere with a radius of 3 voxels to close small holes in the skull, resulting in the binary image  $S(x)$  of the solid skull volume  $\Omega_S$ .

### 2.2. Target head surface reconstruction

The head surface associated to a given target skull is reconstructed in three steps (Fig. 1). First, all reference skulls are non-linearly warped to the target skull. Second, these warps are applied to all the associated reference heads. Finally, a, possibly weighted, average of these warped reference heads is proposed as the final reconstruction of the target head. The crux of the proposed method lies in the particular selection of the warping function in combination with an appropriate representation of the skulls and heads to be non-linearly aligned. The warping should result in a robust and relatively precise deformation of the reference skulls to the target skull. At the same time this deformation should smoothly extrapolate outwards to provide acceptable deformations of the head surfaces. Traditional warping methods first determine a set of corresponding points  $\{p_i^r, p_i^t\}$  on the reference and target surfaces  $S^r$  and  $S^t$  to be warped to each other and then define a warping or coordinate transformation function  $f(p^r) = p^t$  aligning the two point sets while at the same time spatially inter- and extrapolating the warping. Thin-plate splines (TPS) are typically used for the coordinate deformation function  $f$ . They interpolate or approximate the deformation function at the two point sets  $\{p_i^r, p_i^t\}$ , and provide a maximally smooth, in some sense a geometrically simplest, transformation in between the points.

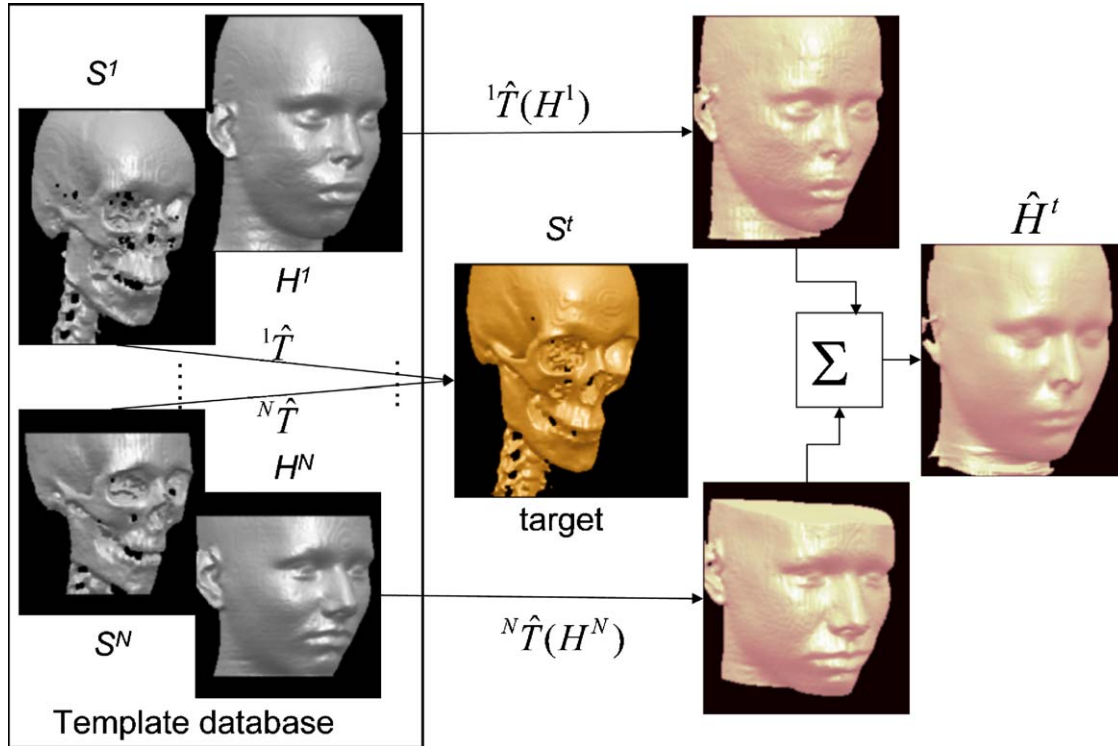


Fig. 1. Flow chart of reconstruction method. See the text in Section 2.2 for further details.

In order to better control the deformation away from the skull surfaces that define the warping, we propose to calculate the coordinate deformation function  $f$  in a higher dimensional space, that is, we represent the surfaces  $S$  as isosurfaces  $S = \{x | s(x) = c\}$  of an implicit 3D embedding function  $s(x): R^3 \rightarrow R$  and rephrase the estimation of the surface warping into the estimation of a 3D deformation field  $f(x)$  between the two implicit functions (or images)  $s^r(x)$  and  $s^t(x)$ . More particularly, we choose the 3D embedding function  $s(x)$  to be a monotonic function of the distance of  $x$  to the surface  $S$ . These 3D embedding functions not only code the original surfaces  $S$  as their zero-level sets  $S = \{x | s(x) = 0\}$ , but, at the same time, code an infinite set of surfaces  $S_c = \{x | s(x) = c\}$  which are smoothed versions of the original surface  $S$ . As a result, the warping  $f$  of these embedding functions will also be influenced by the surface clones at progressively larger distances. This property is particularly interesting in our application since we want to infer the deformation at a distance away from the skull surface.

More formally, the binary images  $S$  and  $H$  corresponding to the volumes  $\Omega_S$  and  $\Omega_H$  encompassed by the external surfaces of skull and head, respectively, are transformed into distance images  $D_S, D_H$  using a signed distance transform (sDT). These images represent for each voxel position  $x$  the shortest distance to the nearest surface point, with a negative sign for voxels outside and positive inside the (closed) surfaces:

$$D_f(x) = \begin{cases} \min_{y \notin \Omega_f} |x - y|, & x \in \Omega_f \\ -\min_{y \in \Omega_f} |x - y|, & x \notin \Omega_f \end{cases}$$

The 3D embedding functions, represented as 3D images  $D_f$ , are non-rigidly aligned to each other using a B-spline based free

form deformation (FFD), which deforms the image by manipulating a regular lattice  $L$  of control points that spans the embedding space. The deformation  $T$  is represented by three coordinate transformations, mapping the  $x, y$  and  $z$ -coordinate value of a point in one image to its corresponding coordinate value in the other image. The deformation is defined at the lattice control points and interpolated in between using a piecewise cubic polynomial function. As a result, local transformations can be modelled in a computationally efficient way, in contrast to the thin plate splines that have more global characteristics and are numerically inferior for large numbers of, especially regularly positioned, landmark points. In order to preserve the regularity of the deformation, additional smoothing constraints are imposed, penalizing excessive bending and excessive local shrinkage or expansion (see [16] for more details). The deformation is estimated by maximizing a similarity criterion between the target image  $D^t(x)$  and the deformed reference image  $D^r(T(x))$ . The similarity criterion is a functional of the two images that returns a real number estimating how well the two images are alike. We have chosen a statistical criterion, mutual information (MI), that measures the statistical dependence between the intensities of the corresponding voxels in the two images and that has been shown to perform well in multi-dimensional linear and non-linear image registration [17,18]. The particular choice of implementation parameters (the resolution of the control lattice, the number of sub-divisions of the control lattice, the relative importance of the smoothing constraints, the numerical optimization parameters, the numerical procedure for calculating MI, etc.) for this application was based on a limited pilot study in which the whole registration procedure (including the head reconstruct-

tion) was visually evaluated for a small subset of parameter values.

Finally, given a target skull  $S^t$ , an estimate of the associated head surface  $\hat{H}^t$  is obtained as follows. The sDT map  ${}^iD_S^t$  of every reference skull  $S^r$ ,  $i = 1, \dots, N$  in the database, is non-linearly transformed to the sDT map  $D_S^t$  of the target skull resulting in transformations  ${}^i\hat{T}$ ,  $i = 1, \dots, N$ . These transformations are subsequently applied to the reference head surface sDT maps  ${}^iD_H^r$ :

$${}^i\hat{D}_H = {}^iD_H^r({}^i\hat{T}(x)), \quad i = 1, \dots, N$$

Since the transformations we obtain are constrained to be smooth, the deformed sDT maps are still close to the signed distance map of the deformed surface. As a result, we can use the shape blending procedures proposed in the computer graphics community [19] to generate new shapes  $S$  interpolating between two or more parent shapes  $S^1$  and  $S^2$ , by simply interpolating their implicit function representations  $s^1(x)$  and  $s^2(x)$  as follows:

$$s(x) = \alpha s^1(x) + (1 - \alpha)s^2(x),$$

with the average shape obtained by setting  $\alpha = 0.5$ . The interpolated surface  $S$  is then defined by  $S = \{x | s(x) = 0\}$ . Applying this implicit surface interpolation scheme, we obtain a statistically plausible target head surface  $\hat{S}^t$  as the zero-value isosurface of the arithmetic mean of the aligned reference head surface sDT maps  ${}^i\hat{D}_H$ :

$$\hat{S}^t = \left\{ x \mid \left( \sum_i^N {}^i\hat{D}_H(x) \right) / N = 0 \right\}.$$

### 2.3. Validation

We evaluate this reconstruction procedure using a leave-one-out test as follows. Each subject in the database is selected in turn as the target and reconstructed from the remaining reference subjects. The reconstructed head surface can then be compared to the real head surface, both visually and quantitatively. The distance  $D$  between the original and the reconstructed head surface is defined as the unsigned distance between corresponding points on both surfaces, averaged over all points. In order to compare head surfaces of different subjects, we use a coordinate system-free representation of surface  $S$  [20] as the set of Euclidean distances between all pairs of points  $p_i$  and  $p_j$  ( $i, j = 1, \dots, K$ ) on surface  $S$ , stored in the Euclidean distance matrix (EDM)  $E_S$  of the surface  $S$ :  $E_S(i, j) = \|p_i - p_j\|$ . Note that we only need to store the  $L = K(K - 1)/2$  upper-triangular elements, the matrix  $E_S$  being symmetric with zeroes on the main diagonal. The EDM representation is interesting since it is invariant to translations and rotations of the surface. The distance  $D$  and the EDM  $E$  are evaluated for a subset of 500 surface points selected randomly but evenly on a reference head surface  $S^R$ . This reference surface was constructed as the average of 118 faces not in the database used for this project [12]. The corresponding points on every head surface, both original and reconstructed, are defined

by deforming this reference surface to all the head surfaces using a variant of the iterative closest point (ICP) non-rigid surface-based registration algorithm [12].

We use the EDM representation to compare every reconstructed head surface to every original head surface. The comparison uses a distance functional that returns a real number reflecting the degree to which two surfaces are dissimilar. In this study we used the sum of squared differences (SSD) between corresponding elements in the EDM  $E_S^1$  and  $E_S^2$  of the two surfaces  $S^1$  and  $S^2$ :

$$\|E_S^1 - E_S^2\| = \sum_{i,j>i} \left( E_S^1(i, j) - E_S^2(i, j) \right)^2 / L$$

This measure is zero for identical surfaces and is strictly positive for dissimilar surfaces. Ideally, the more similar two surfaces are, the smaller this measure is. Since the EDM representations are invariant to rotation and translation, we do not need to geometrically align the two surfaces before comparison. In order to be invariant to scaling as well, we also calculate the same distance measure but now between the EDM representations  $N_S$  normalized for size. Following [20], we divide each element in the EDM representation  $E_S$  by the geometric mean of all EDM elements of  $E_S$ :  $N_S(i, j) = E_S(i, j) / \gamma(E_S)$ , with  $\gamma(E_S) = (\prod_{ij} E_S(i, j))^{1/L}$ . The SSD between the two normalized EDM representations  $N_S^1$  and  $N_S^2$  then provides a distance measure comparing two surfaces irrespective of their size.

Using both distance measures we can generate a classification rank matrix, ordering for each reconstructed head surface all original surfaces in ascending distance order. Perfect classification would then result in the correctly corresponding original surface being ranked one for every reconstruction. We report results for both distance measures as the number of reconstructions classified correctly in rank 1, rank 1 or 2, etc. We expect that the classification results using the normalized measure will be inferior to the results obtained using the non-normalized measure, since size may be a highly discriminative feature in comparing head surfaces of different subjects.

## 3. Results

### 3.1. Image pre-processing and segmentation

Fig. 2 shows an axial cross-section of the CT-image at a level containing severe metal streak artefacts due to amalgam tooth fillings, before and after metal artefact reduction (MAR), together with the associated 3D renderings of the skull and head surfaces. While most of the high intensity part of the artefact that interferes with the bone segmentation has been removed, parts near the high-density material still remain.

### 3.2. Craniofacial reconstructions

Fig. 3 shows the different steps for an individual subject. The left column shows a lateral and frontal view of the 3D surfaces of skull and head of a reference subject in the database. The

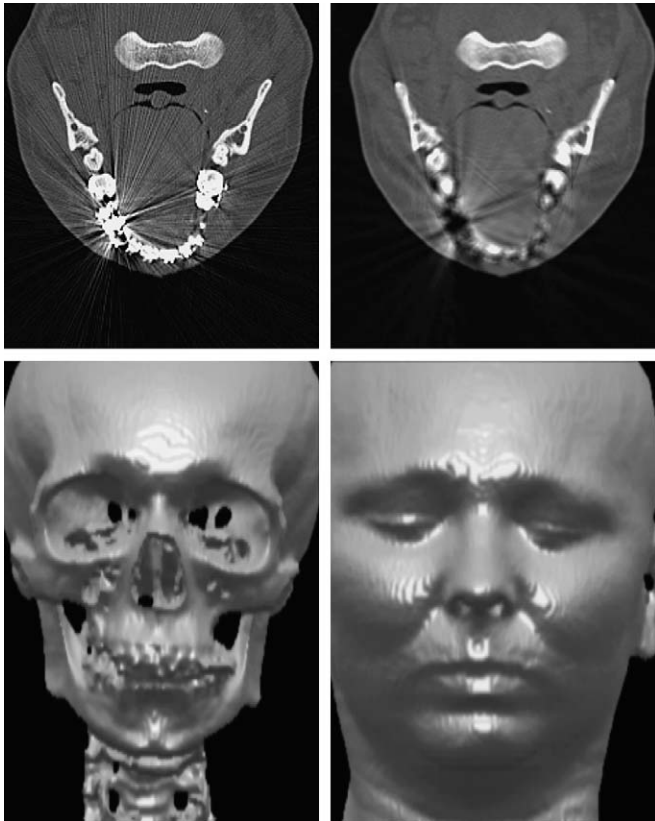


Fig. 2. Pre-processing and segmentation example. Top row: axial cross-sections before (left) and after (right) metal artefact removal (MAR). Bottom row: 3D surface rendering of segmented skull and head volume after MAR.

middle column shows the deformed reference skull and head surface. The deformation is such that the resulting skull surface matches as well as possible the target skull surface. The right column shows the corresponding views of the target subject.

Figs. 4 and 5 show all 20 cases reconstructed. A three-quarter surface view of the original head surface (first and third column) and the corresponding reconstructed head surface (second and fourth column) are displayed. By comparing original and reconstructed surfaces, we observe that the overall shape of the head has been largely recovered except for detailed surface parts such as the nostrils and the lips. Note that the reconstructions are constructed as pure arithmetic averages of the deformed reference head surfaces without any specification of gender, age or body mass index. As a result, the reconstructions do not exhibit any age, sex or body posture related characteristics.

### 3.3. Quantitative validation

Fig. 6 shows the spatial distribution of the average values and the standard deviations of the reconstruction error, defined as the shortest unsigned distance between the original and the reconstructed surface at that point, for all 20 subjects, projected onto the average facial template. The overall average and standard deviation of the reconstruction error, integrated over the complete facial template, is 1.9 and 1.7 mm, respectively. The larger reconstruction errors (2–3 mm on average) occur at

the nostrils and the masseter region. While the average and standard deviation reveal the general aspects of the reconstruction procedures, Fig. 7 shows the reconstruction error for two qualitatively different reconstructions. The figure at the top left (corresponding to the subject shown in Fig. 5 second row, third and fourth column) shows a relatively small (<2 mm) overall reconstruction error, while the image at the bottom left (corresponding to the subject shown in Fig. 4 second row, third and fourth column) exhibits large (6 mm) errors in the masseter region and both sides of the upper forehead (>3 mm). In the latter case, the unexpectedly large errors on the forehead are artificial since the subject's face was incompletely scanned, the field of view extending to just above the eyebrows. The missing facial surface parts are estimated as pure extrapolations from information inside the scanned part. The difference in scanning area for the two subjects is shown in the figures on the right.

Using the non-normalized distance measure  $\|E_S^1 - E_S^2\|$  between every reconstructed and every original head surface, we found the correctly corresponding face ranked number 1 in 70% of the cases, in top rank 2 in 80% and in top rank 3 in 85% of the cases. Using the normalized distance measure  $\|N_S^1 - N_S^2\|$  these numbers dropped to 65%, 70% and 80%, as expected, since the size of a face, coded implicitly in the non-normalized EDM representations, is an additional distinguishing feature, not available in the scale-invariant normalized distance measure. Parallel tests using the linear correlation coefficient between the EDM elements as a similarity test showed similar results.

## 4. Discussion

Traditionally, facial soft tissue depths have been measured using needle puncturing on cadavers. Poor relationships have been reported between cadaver-based and in vivo measurements, due to tissue deformation after post-mortem changes, such as dehydration and shrinkage or even swelling with the onset of putrefaction. The accuracy of the tissue depth data as well as the sampling density improved with the arrival of in vivo, non-invasive depth measurements such as lateral cephalometric radiography, ultrasound, magnetic resonance imaging and CT-scanning. Ideally, one could obtain densely sampled facial soft tissue measurements very easily from 3D X-ray CT scans due to the excellent image contrast of bone versus soft tissue and soft tissue versus air. Moreover, the recent introduction of multi-slice spiral or helical CT reduced scanning time as well as patient radiation dose while generating images with a higher transaxial spatial resolution. However, acquisition of such data sets over a sufficiently large, representative, normal (!) population is ethically improbable because of the remaining radiation dose still involved. As a result we are limited to the use of existing patient databases of clinical CT scan protocols.

Kim et al. [21] studied the precision and accuracy of CT-based facial soft tissue depth measurements on cadaver heads, using a PC-based interactive measurement procedure on multi-planar reformatted (MPR) views. Various CT scanning protocols were compared to measurements obtained by

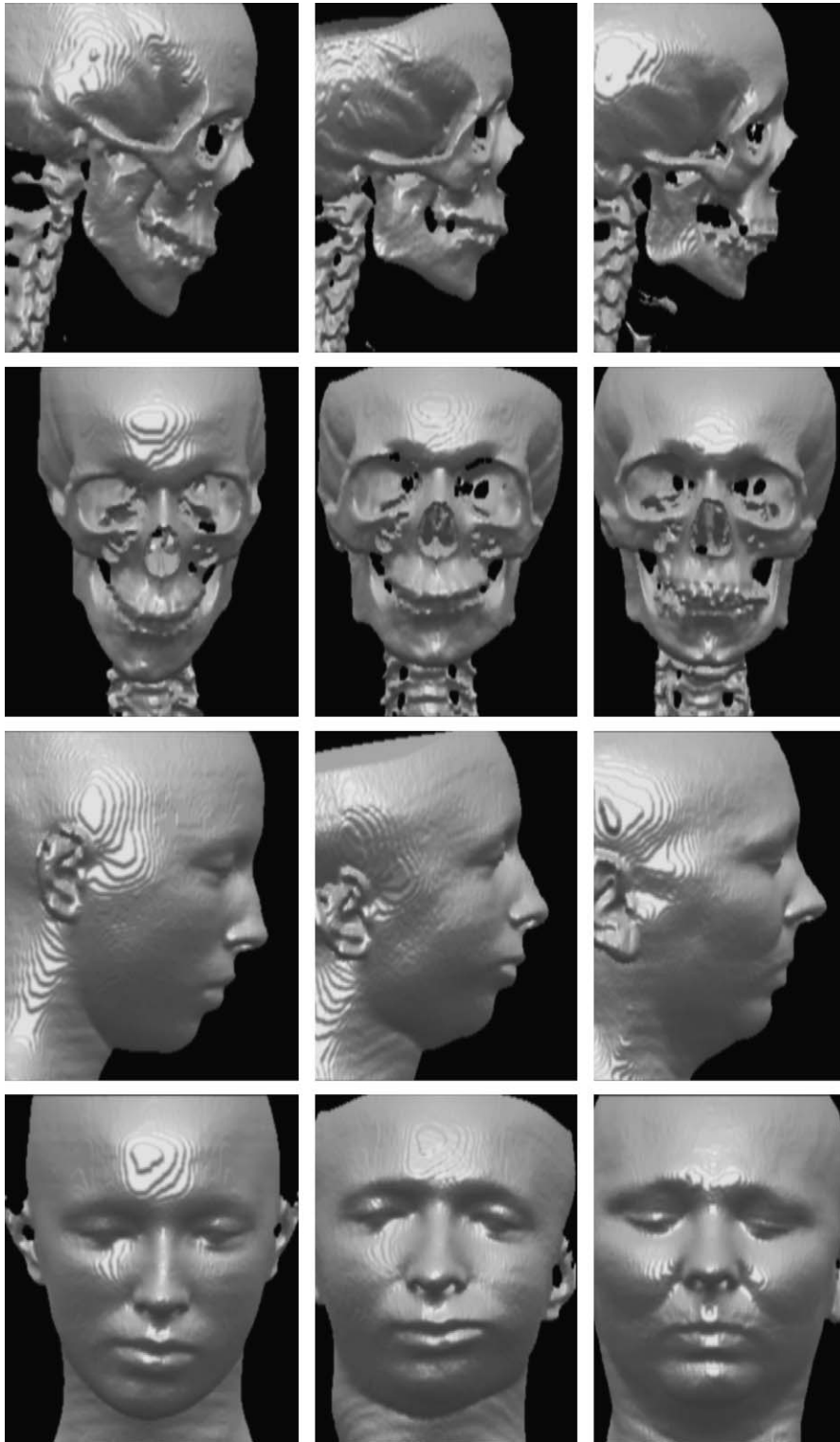


Fig. 3. Example deformation (lateral and frontal 3D surface view) from reference subject (left column) to target subject (right column). Warped reference skull and skin surfaces are shown in the middle column.

physical puncturing. They concluded that “PC-based MPR CT images of the face using routine scanning CT protocols can be used to accurately measure soft tissue thickness in the facial region”. In a similar vein, De Greef et al. [22] compared ultrasound-based measures to multi-slice spiral CT based

measures on 12 subjects, showing only statistically significant differences for landmarks located in the masseter region. These differences were attributed to the differences in positioning (upright for ultrasound-based measurements, supine for CT-based measurements). From these studies, we conclude that

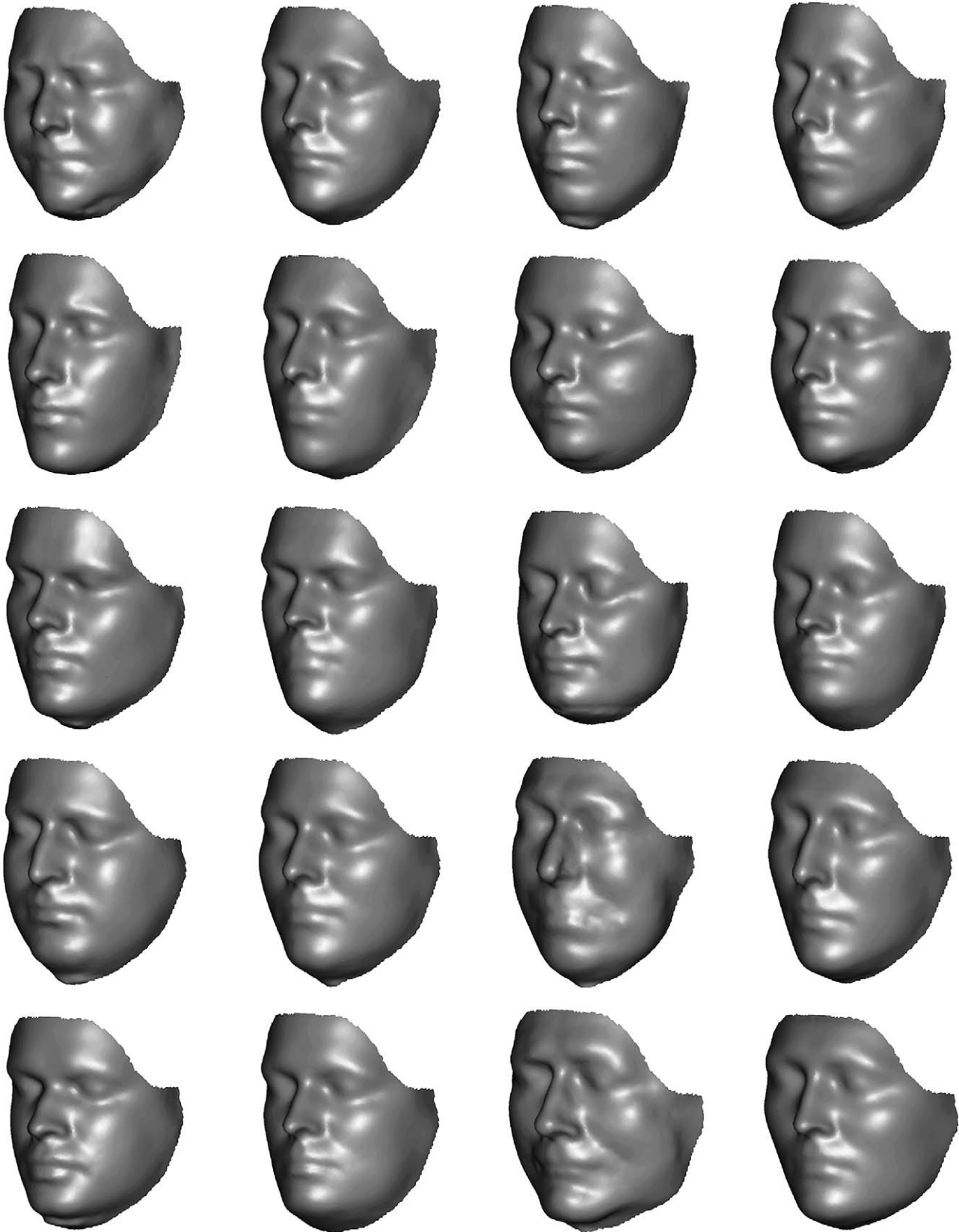


Fig. 4. Leave-one-out head reconstructions of subjects 1–10. First and third column: original head surface. Second and fourth column: reconstructed head surface from remaining 19 subjects.

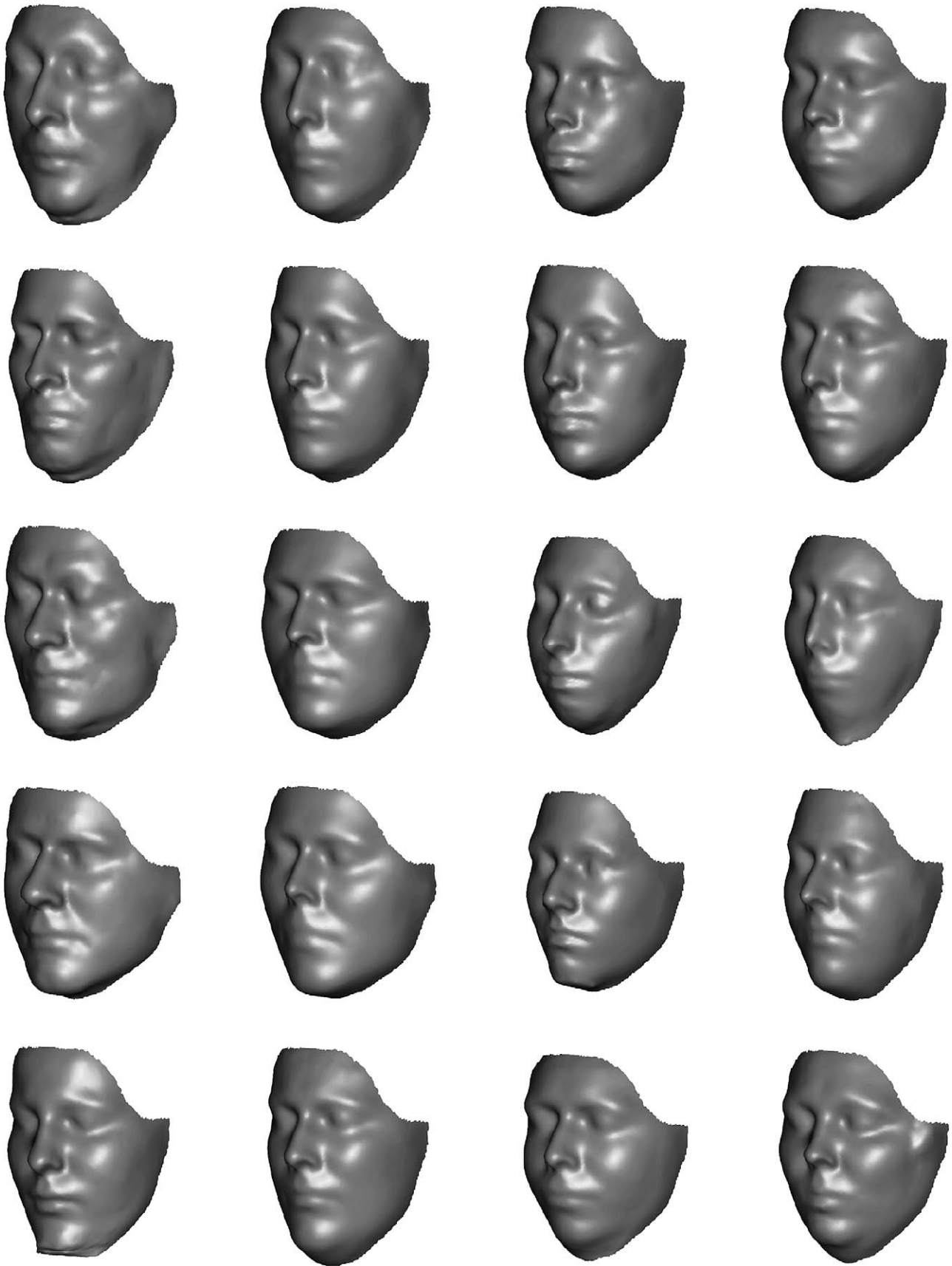


Fig. 5. Leave-one-out head reconstructions of subjects 11–20. First and third column: original head surface. Second and fourth column: reconstructed head surface from remaining 19 subjects.

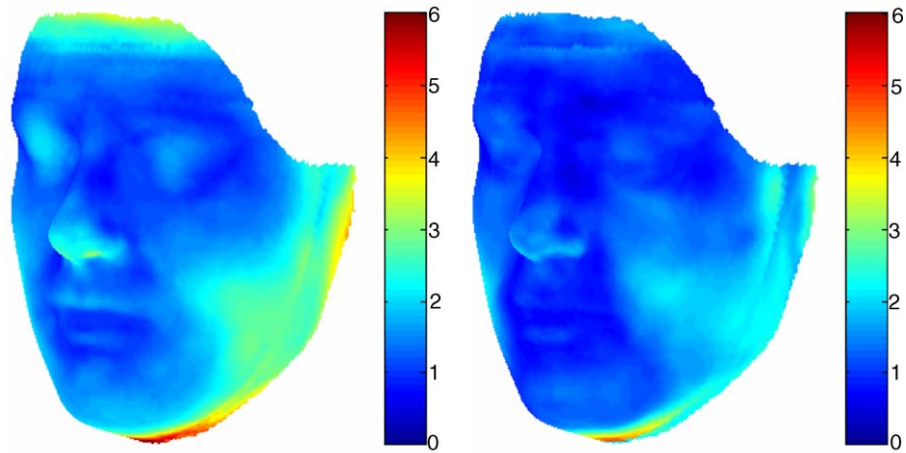


Fig. 6. Average (left) and standard deviation (right) absolute reconstruction errors for all 20 subjects mapped onto an average facial template. Errors are measured in mm.

CT-imaging offers the possibility to reliably and accurately measure facial soft tissue depths.

The inherent accuracy of CT images can, however, be jeopardized at the level of the teeth by the presence of metal streak-like artefacts due to amalgam teeth fillings. The metal artefact removal (MAR) procedure implemented in this study is

not completely successful in removing the high intensity artefacts that interfere mostly with the intensity thresholding procedures for the bone structures. Although morphological filtering can remove most of these artefacts, too much of the regular bone structure morphology risks to be changed as well. Implementation of more sophisticated MAR procedures is thus

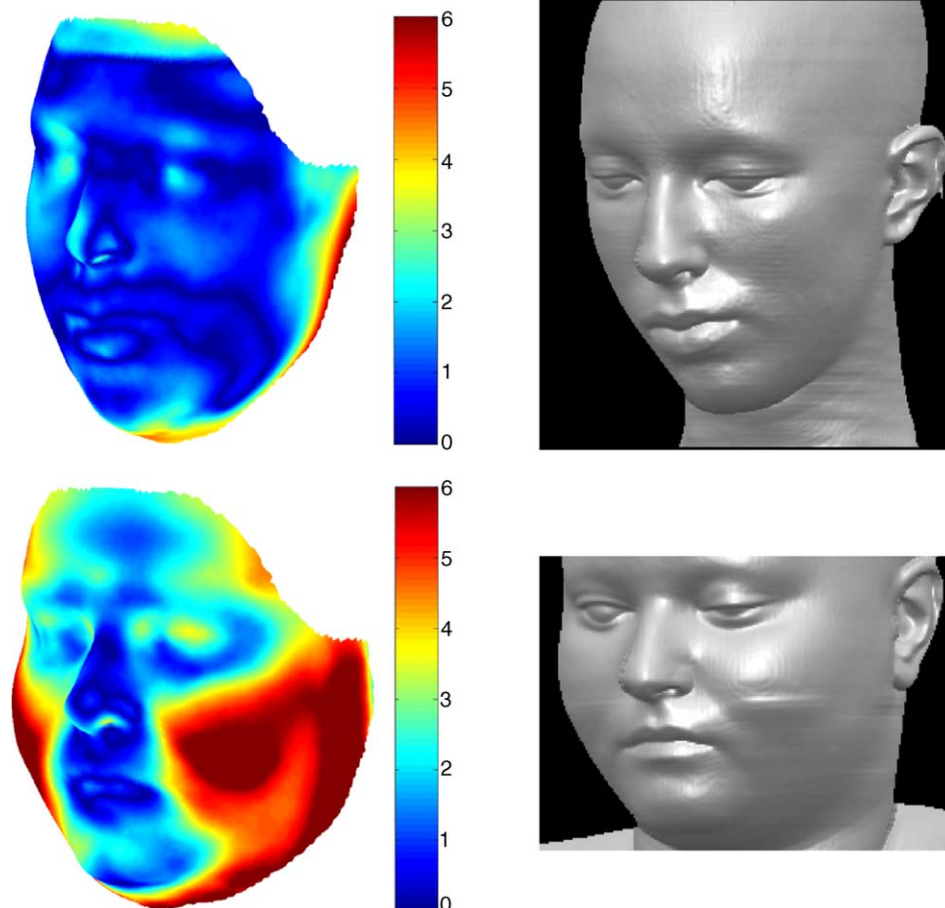


Fig. 7. Reconstruction error for two individual cases showing a large spectrum of reconstruction errors. The errors are plotted on the original head surfaces (left). Errors are measured in mm. Right: 3D surface rendering of corresponding original head surfaces, showing differences in scanning area.

required for the construction of a large enough reference database for craniofacial reconstruction. Alternatively, warping procedures less susceptible to the presence of these anatomically implausible structures could be envisaged, for instance, by incorporating statistical deformation models, as will be discussed infra.

The non-rigid registration algorithm that we proposed in this paper to warp the implicit surface representations of the reference skull  $D_S^r$  to the target skull  $D_S^t$ , optimizes a similarity criterion over the parameters (the vector displacements of the B-spline lattice control points) that define the transformation  $T$ . The particular choice of signed distance transforms for the surface representations could have suggested a similarity functional based on the squared differences of the signed distance values, summed over all voxels in the common overlap region of both implicit representations as:

$$\hat{T} = \arg \max_T \sum_x \left( D_S^t(x) - D_S^r(T(x)) \right)^2$$

This would align the implicit representations such that the distances of the target image and the warped distances of the reference image are as similar as possible. However, we have chosen mutual information (MI) as the similarity criterion since it is invariant to monotonic transformations of the intensities in the two input images, such as linear intensity scaling. This is particularly interesting in our context when coping with geometrical scale variations as coded in the implicit surface representations. Indeed, if  $\alpha$  is a global scaling factor,  $T(x) = \alpha x$ , then the implicit representations are transformed as  $s_T(T(x)) = \alpha s(x)$ , and, since MI is invariant to monotonic intensity transformations,  $\text{MI}(s^1(x), s^2(x)) = \text{MI}(s^1_T(T(x)), s^2(x))$ . As a result, MI intrinsically copes with scale variations, which is especially important in the first iterations of the warping procedure, when more global deformations, and hence also the larger scaling variations, are estimated.

Registration of the skull signed distance transforms (sDT) instead of the binary segmentations of the skull has some immediate advantages, since it uses a spatially extrapolated representation of the skull shapes. Because we apply the estimated reference-to-target skull deformation to the skin surface (or its implicit sDT representation), a reliable extension of the deformation is required. The use of the implicit representation in combination with a non-linear deformation model with a limited number of degrees of freedom (about 400 in our study) seems to result in an acceptable reconstruction procedure. However, a more localized non-linear registration procedure is probably required to fine tune to skeletal surface details. We acknowledge that more test cases need to be processed to examine the joint effect of the surface representation and non-linear registration procedure. This could be set up as a global search for that particular choice of intrinsic parameters of the algorithm (number of lattice points, number of levels, ...) that optimizes the reconstructions in the reference database in a leave-one-out scenario. Time and resource constraints have prevented us from performing this large-scale study as yet.

The reconstructions are currently obtained as mere arithmetic averages of the warped reference head sDTs. Linear convex combinations of sDT maps have been used in computer graphics applications for continuous morphing the shape of one structure into another. However, the set of sDTs is not closed under linear combinations, meaning that a linear combination of sDTs is not necessarily a true sDT of the embedded surface. Other implicit functions can be suggested (e.g. any monotonic function of the original Euclidean distance or solutions to variational problems, such as radial basis function representations), but the Euclidean sDT is very simple in implementation and has an intuitive interpretation. Non-linear warping of an sDT further distorts the representation of true distances to the embedded surface. However, as long as the warping remains smooth and locally small in magnitude, as is the case in the proposed method, warped sDTs can be assumed to be fair approximations to the sDT of the warped embedded surface. The relationship between surface warping and implicit function representations requires further investigation, though.

Combinations other than the arithmetic average can be suggested. For instance, the linear weights for the warped skin sDTs could be made dependent on the similarity of the warped skull to the target skull (for instance their relative amount of overlap after warping). Initial experiments on weighted combinations of linearly warped skin sDTs showed only minor changes compared to the simple average, mainly because the similarity measure used was not sensitive enough and not specific for the parts of interest (it measured the relative overlap of bone regions over the whole head and not just the frontal facial part). Following the work of Claes et al. [12] and Tu et al. [13], instead of reporting only the average of all warped skin sDTs, in addition, major modes of variation could be reported as well. This requires a large enough reference data set for the statistical variations to be representative. Such a data set would also allow weighing of the combinations towards class-similar surfaces (same gender, age, and body mass index). Finally, weighing is now implemented globally, all points on the surface (or embedding sDT) being considered equal. Local weighing schemes could improve particular features, such as the nose, eyes and lips, by only taking local correlations into account.

The proposed reconstruction procedure uses a dense, almost continuous, sampling of soft tissue depths over the complete face. It is, to the best of our knowledge, also the first such study that goes beyond the presentation of single cases by providing an, admittedly, small-scale ( $N = 20$ ) quantitative validation. In this validation we used one particular similarity measure, the sum of squared differences between the corresponding matrix elements of the normalized/non-normalized EDM representations of two surfaces. Other similarity measures, such as Procrustes distances between corresponding surface points, can be defined and will probably generate slightly different classification results. Anyhow, we believe that the proposed validation procedure is only a first but necessary, since well controlled, step in the overall validation of the reconstruction algorithm.

While the results of this pilot study are promising, further improvements can be expected especially by extending the reference database in conjunction with attribute-specific

selection or weighing in combining the warped reference images. Our procedure is completely automatic and does not require explicit point correspondences between homologous anatomical points on the skulls. This unfortunately also implies that it will occasionally, but inevitably, make errors in warping two different skulls because of the lack of anatomical guidance. We conjecture that a combination of this implicit dense ( $N > 10,000$ ) warping procedure with the sparse ( $N < 100$ ) anatomical landmark based procedures as presented by Claes et al. [12] will result in a more complete and robust reconstruction procedure. We must finally acknowledge that the success of any such procedure should eventually be measured in a suitable forensic context, for instance, by setting up a well-designed validation procedure such as face-pool testing.

## 5. Conclusion

We have presented a fully automatic procedure for craniofacial reconstruction, using a database of reference head CT scans. All reference images are automatically segmented into head volumes (enclosed by the external skin surface) and bone/skull volumes, both represented by a signed distance transform (sDT) map. The reference skull sDTs are (non-)linearly warped to the target skull sDT and this warping is applied to all reference skin sDTs. A linear combination of the warped reference skin sDTs is proposed as the reconstruction of the external skin surface of the target subject. Results on a pilot reference database ( $N = 20$ ) show the feasibility of this approach, although further investigations are required. First, metal streak artefacts need to be removed from the images, since they possibly distort the reconstructions to an unacceptable extent. Second, the warping procedure needs to be examined more carefully, paying attention on the one hand to better fitting of reference to target skull and smooth extrapolation of the warping on the other hand. Third, other linear combinations besides the mere average need to be explored. Finally, a more extensive quantitative validation framework for the reconstructions needs to be set up.

## Acknowledgements

This work is supported by the Flemish Institute for the Promotion of Innovation by Science and Technology in Flanders (IWT, project IWT/GBOU/020195), by the K.U. Leuven (project/OF/GOA/2004/05) and by the Fund for Scientific Research—Flanders (FWO-Vlaanderen, projects FWO/G.0258.02 and FWO/G.0566.06). The authors also acknowledge the support of Dr. Hermans (Department of Radiology, University Hospitals Leuven, Belgium) and Dr. Nadjmi (Eeuwfeest Clinic, Antwerpen, Belgium) in providing the CT data.

## References

[1] J. Prag, R. Neave, *Making Faces using Forensic and Archaeological Evidence*, British Museum Press, 1997.

- [2] K.T. Taylor, *Forensic Art and Illustration*, CRC Press, New York, 2001.
- [3] R. Evenhouse, M. Rasmussen, L. Sadler, Computer-aided forensic facial reconstruction, *J. Biocommun.* 19 (1992) 22–28.
- [4] A.W. Shahrom, P. Vanezis, R.C. Chapman, A. Gonzales, C. Blenkinsop, M.L. Rossi, Techniques in facial identification: computer-aided facial reconstruction using laser scanner and video superimposition, *Int. J. Legal Med.* 108 (1996) 194–200.
- [5] A.J. Tyrell, M.P. Evison, A.T. Chamberlain, M.A. Green, Forensic three-dimensional facial reconstruction: historical review and contemporary developments, *J. Forensic Sci.* 42 (1997) 653–661.
- [6] P. Vanezis, Application of 3D computer graphics for facial reconstruction and comparison with sculpting techniques, *Forensic Sci. Int.* 42 (1989) 69–84.
- [7] P. Vanezis, M. Vanezis, G. McCombe, T. Niblet, Facial reconstruction using 3D computer graphics, *Forensic Sci. Int.* 108 (2000) 81–95.
- [8] M.W. Jones, Facial reconstruction using volumetric data, in: T. Ertl, B. Girod, H. Niemann, H.-P. Seidel (Eds.), *Proceedings of the 6th International Vision Modelling and Visualisation Conference—VMV-01*, vol. 21–23, Stuttgart, Germany, 2001, pp. 135–150.
- [9] L.A. Nelson, S.D. Michael, The application of volume deformation to three-dimensional facial reconstruction: a comparison with previous techniques, *Forensic Sci. Int.* 94 (1998) 167–181.
- [10] G. Quatrehomme, S. Cotin, G. Subsol, H. Delingette, Y. Garidel, G. Grevin, M. Fidrich, P. Baillet, A. Ollier, A fully three-dimensional method for facial reconstruction based on deformable models, *J. Forensic Sci.* 42 (1997) 649–652.
- [11] G. Subsol, G. Quatrehomme, Automatic 3D facial reconstruction by feature-based registration of a reference head, in: J.G. Clement, M.K. Marks (Eds.), *Computer-graphic Facial Reconstruction*, Elsevier Academic Press, 2005, pp. 79–101.
- [12] P. Claes, D. Vandermeulen, S. De Greef, G. Willems, P. Suetens, Statistically deformable face models for craniofacial reconstruction, in: S. Lončarić, H. Babić, M. Bellanger (Eds.), *Proceedings of the 4th International Symposium on Image and Signal Processing and Analysis—ISPA2005*, Zagreb, Croatia, September 15–17, (2005), pp. 347–352.
- [13] P. Tu, R. Hartley, W. Lorensen, M. Allyassin, R. Gupta, L. Heier, Face reconstruction using flesh deformation modes, in: J.G. Clement, M.K. Marks (Eds.), *Computer-graphic Facial Reconstruction*, Elsevier Academic Press, 2005, pp. 145–162.
- [14] J. Wei, L. Chen, G.A. Sandison, Y. Liang, L.X. Xu, X-ray CT high-density artefact suppression in the presence of bones, *Phys. Med. Biol.* 40 (2004) 5407–5419.
- [15] R. Gonzalez, R. Woods, *Digital Image Processing*, 2nd ed., Prentice Hall, 2002.
- [16] D. Loeckx, F. Maes, D. Vandermeulen, P. Suetens, Non-rigid image registration using free-form deformations with a local rigidity constraint, *Lect. Notes Comput. Sci.* 3216 (2004) 639–646.
- [17] F. Maes, A. Collignon, D. Vandermeulen, G. Marchal, P. Suetens, Multimodality image registration by maximization of mutual information, *IEEE Trans. Med. Imaging* 16 (1997) 187–198.
- [18] X. Huang, N. Paragios, D. Metaxas, Registration of Structures in Arbitrary Dimensions: Implicit Representations, Mutual Information and Free-form Deformations, Technical Report DCS-TR-0520, Division of Computers and Information Science, Rutgers University, 2003.
- [19] B. Payne, A. Toga, Distance field manipulation of surface models, *IEEE Comput. Graph. Appl.* 12 (1992) 65–71.
- [20] S.R. Lele, J.T. Richtsmeier, *An Invariant Approach to Statistical Analysis of Shapes*, Chapman & Hall/CRC, 2001.
- [21] K.D. Kim, A. Ruprecht, G. Wang, J.B. Lee, D.V. Dawson, M.W. Vannier, Accuracy of facial soft tissue thickness measurements in personal computer-based multi-planar reconstructed computed tomographic images, *Forensic Sci. Int.* 155 (2005) 28–34.
- [22] S. De Greef, P. Claes, W. Mollemans, M. Loubele, D. Vandermeulen, P. Suetens, G. Willems, Semi-automated ultrasound facial soft tissue depth registration: method and validation, *J. Forensic Sci.* 50 (2005) 1282–1288.